Conformal Growth of Organic Luminescent Planar Defects within Artificial Opals

Francisco J. Aparicio, Gabriel Lozano, Iwona Blaszczyk-Lezak, Ángel Barranco*, and Hernán Míguez*

Instituto de Ciencia de Materiales de Sevilla (CSIC-US), Avenida Américo Vespucio s/n, Isla de La Cartuja, 41092 Sevilla, Spain

Materials should be requested to hernan@icmse.csic.es and angelbar@icmse.csic.es.

FJA and GL contributed equally to this work.

Herein we present the result of combining, for the first time, the techniques of colloidal self-assembly and plasma enhanced chemical vapour deposition to create a novel, high quality, purely organic active photonic crystal structure of controlled optical properties. We show a fast, reliable and accurate procedure to introduce two dimensional luminescent organic defect layers within artificial polystyrene opals by a versatile room temperature remote plasma deposition process. This method is gentle enough as to allow highly conformal growth on polystyrene microspheres without altering their morphology or the ordered arrangement they form. The luminescent organic layer behaves both as an optical dopant, causing the opening of transmission windows within the forbidden frequency interval of the lattice and as an optically active material, whose emission can be tailored by the photonic environment.

1. Introduction

The controlled introduction of defects within photonic crystals has attracted great attention since the early days of the field.[1] The reason lies mainly in the interest in carefully engineering defect states within the photonic gap of such lattices, in order to attain waveguides of higher performance or slow propagation modes.[2] A number of techniques have also been applied to create both line and planar defects within solid self-assembled photonic crystals made of spherical colloids, also known as artificial opals.[3] Since polymer defect lines in the bulk of a silica opal were first achieved by using a multi-photon confocal laser to selectively induce polymerisation of the embedded monomer,[4] different motifs have been devised and realized within colloidal crystals by a wide variety of techniques,[5,6,7] such as direct laser writing,[8] electron beam lithography,[9,10] photolithography,[11,12] or by modifications of the method originally proposed.[13] Significantly, light transmission through linear air defect channels built up in a silicon inverse opal[14,15] structure has recently been demonstrated.[16]

A few successful approaches have also been taken up to date to introduce planar defects in artificial opals. A layer of spheres of an arbitrary diameter can be introduced within the bulk of an opal by combining colloidal crystal planarization and Langmuir-Blodgett techniques.[17] A combination of

convective self assembly and silicon oxide chemical vapour deposition[18] has been used to create a slab sandwiched between two opal films.[19,20] A procedure based on spin-coating has also been applied to build, in the first place, embedded layers of nanoparticles,[21] and extended later on as a generic method for a variety of materials.[22] This has allowed the observation of slow light modes in controlled defects built in self-assembled photonic crystals for the first time.[23] Transfer printing has also been used to place a polymer multilayer of controlled thickness on top of an opal film, a second opal being grown on top of it afterwards.[24] In this latter case, the optical effects associated to the presence of defects, such as sharp dips (peaks) observed in the reflectance (transmittance) spectra at stop band frequencies, can be precisely tuned through externally induced changes of the polymer material the defect is made of. These structures offer as well the possibility to modify the emission of optically active defect slabs embedded within. In this regard, only one relevant precedent work has reported on the lasing properties of a polymer defect layer containing organic dyes molecules sandwiched between two flexible self-assembled photonic crystals.[25] In order to achieve so, a fluid mixture of an oligomer, a curing agent and dye molecules was infiltrated between two colloidal crystals that had been previously stabilized by infiltration of polydimethilsyloxane (PDMS), which endows mechanical stability and flexibility to the lattice and prevents the luminescent molecules to flow outside the defect layer. A photopolymerization process is then induced by exposure to UV radiation to stabilize the defect layer. This procedure results in high quality photonic structures in which, unfortunately, the refractive index contrast has been largely reduced due to the infiltration of PDMS within the crystals, which diminishes its scattering strength and thus the magnitude of the localization effects associated with the presence of a defect layer.

Here we present a fast, reliable and accurate procedure to create two dimensional luminescent organic defect layers in artificial opals preserving the photonic strength of the lattice. The planar defect is formed by a versatile room temperature remote plasma deposition process that can be used to create mechanically stable and non-soluble coatings of a wide variety of organic compounds. The process is gentle enough as to allow highly conformal growth on polystyrene microspheres without altering their morphology or the ordered arrangement they form, thus giving rise to purely organic photonic nanostructures. Accurate control of the defect thickness is achieved, which yields control over the

spectral position of the defect state introduced in the pseudogap of the photonic crystal due to the breaking of translational symmetry. This resonant mode causes the opening of a narrow transmission window that can be precisely adjusted during the synthesis. The emission properties of the middle layer can be controllably modified through the structural properties of the photonic environment in which it is embedded.

In spite of the great amount of materials that can be grown using plasma based techniques,[26] up to date, they had only been applied for the processing of self-assembled photonic materials as a means to selectively remove an ordered organic matrix that had been used to either mold a guest material or hold a more complex structure together.[27] Most plasma processes are too aggressive both chemically and thermally for organic materials, such as polystyrene opals, to resist them. However, they present a number of advantages that make them extremely desirable to prepare optical coatings, the main ones being probably the strict control of the features achievable at the nanometer scale, the conformal character of the growth and the great reliability and reproducibility of the process. In our case, we have employed a plasma enhanced chemical vapour deposition (PECVD) technique developed at our laboratories,[28,29,30] in which partial polymerization of functional organic molecules is induced by the controlled interaction with a remote microwave plasma. By this methodology it has been possible to deposit a layer of a luminescent organic solid material directly on a polystyrene artificial opal. The luminescent dye 3-hydroxiflavone and adamantane are used as precursor for the synthesis of such films. Since full details are given in the experimental section, suffices to say here that we have achieved deposition conditions mild enough as to leave the photonic crystal substrate unaltered during the process. In addition, the hydrophilic character of the organic thin film surface is achieved by tuning the PECVD parameters at the end of the deposition. This latter process has permitted the deposition of a second layer of opal onto it, giving rise to a photonic crystal in which the translational symmetry is broken by the presence of an intermediate luminescent nanostructured film.

2. Materials and Methods

Fabrication of colloidal crystal films. The growth of colloidal crystals from polystyrene (PS) colloids in deionised water was carried out using a variation of the vertical deposition method developed by Colvin *et al.*[3] For this purpose, commercial PS colloidal particles (IIKERLAT) with an average diameter of 220 nm and 750 nm (polydispersity about 3%) were used. Substrates employed were glass microscope slides (12 mm x 76 mm), which were cleaned with doubly distilled water, acetone, carbon tetrachloride and with a 4:1 volume ratio H_2SO_4/H_2O_2 solution before being dried with a N_2 flow. These substrates were dipped into a cylindrical glass beaker (inner diameter, ca. 25 mm; volume, 25 mL) containing the PS colloidal suspensions (15 mL) with a concentration of 0.04% wt. Then, the beakers were placed in an oven at 50ºC and water was evaporated at a rate of 0.22 mm/h for 3 days, a high quality colloidal crystal being formed on an area of 12 mm x 16 mm of the substrate. Similar conditions were employed to grow a second colloidal crystal on the hydrophilic surface of the corrugated polymeric thin film deposited by PECVD in order to create a planar defect embedded in a photonic crystal.

Plasma polymerization of organic layers. The experimental set-up used for deposition of the polymeric thin films consists of a vacuum chamber with two zones for the plasma and for the remote deposition. A set of magnets surrounding the plasma chamber sustain a discharge under microwave electron cyclotron resonance (ECR) conditions. The microwave is applied to the plasma chamber through a flat Pyrex window. The system is fitted with a set of Knudsen cells to sublimate the dye in the deposition zone and a precursor dosification system that can be heat up. The pressure of the system was controlled by an automatically regulated pressure controller connected to a capacitance pressure gauge (Baratron). Argon plasma gas is dosed to the plasma chamber using a calibrated mass flow controller (MKS). The system was pumped before and after deposition with a turbomolecular pump to achieve a base pressure of ~10^{-7} mbar. One side polished Si(100) wafers, quartz, slides and the colloidal crystal films used as substrates were placed in the deposition chamber.

The polymerized thin films were deposited at room temperature by the simultaneous sublimation of 3-Hydroxyflavone and adamantane powders (Aldrich) in the downstream region of an Ar plasma. Film thickness and evaporation rate are controlled by using a quartz crystal monitor placed besides the

sample holder in the deposition region. Typical growing rates between 2-4 nm/min were achieved by controlling the temperature of both the Knudsen cells for the dye and the dosification system for the adamantane. By using relatively low growth rates it was possible to control efficiently the deposition of ultrathin films typically in the range of 20-500 nm. The microwave power was ~150 W and the argon pressure ~$1x10^{-2}$ mbar. Artificial opal samples were located at ~6 cm of the plasma source. Additional details of the experimental set-up used can be founded in Refs. 28-31. Absorbance and fluorescence spectra of 3HF-adamantane plasma polymer film grew over quartz are provided as supporting information. In addition, a complete study of the properties of the 3-HF-adamantane plasma polymers deposited by this novel process will be presented elsewhere.[31] Films were exposed to an oxygen plasma (240 W, 10^{-3} mbar) by introducing an oxygen flow during ~3 minutes at the end of the deposition in order to obtain highly hydrophilic surfaces. Special care was taken not to etch the polystyrene spheres at this stage. Micrographs of top views and cross sections of the different samples prepared were obtained using a Hitachi S5200 field emission scanning electron microscope.

Optical spectroscopy. Optical characterization was performed using a Fourier Transform Infrared Spectrophotometer (BRUKER IFS-66) attached to a microscope and operating both in reflection and transmission mode. For reflectance measurements, an X4 objective with a numerical aperture of 0.1 (light cone angle ±5.7º) was used to irradiate the sample and collect the reflected light at quasi-normal incidence with respect to the (111) planes of the colloidal lattice. A spatial filter was used to selectively detect light from 0.1 mm^2 circular regions of the sample.

Luminescence spectroscopy. Fluorescence spectra were measured in a Jobin-Yvon Fluorolog3 spectrofluorometer equipped with a 450 W Xe lamp using grids of 0.4 and 1 nm for the excitation and emission, respectively. The excitation wavelenght was 350 nm. Fluorescence spectra were measured with slightly modified front-face configuration in order to collect emission spectra at quasi-normal direction with respect to the (111) planes of the colloidal lattice. For this analysis the luminiscent layers were also deposited in quartz slides.

3. Results and discussion

Figures 1 and 2 show different images of the materials prepared as viewed under a field emission scanning electron microscopy (FESEM). Figures 1(a) and 1(b) display images of the top surface of a polystyrene opal (average sphere diameter 220 nm) before and after being coated with the plasma polymeric thin film, respectively. The coherent corrugation of the colloidal crystal substrate is preserved, which demonstrates the highly conformal deposition of the organic thin film that takes place by the PECVD technique employed. The pictures of the cross section taken at different magnifications, shown in Figures 1(c) and 1(d), revealed that the films develop a columnar structure and that the growth occurs preferentially from the surface of the microspheres upwards. Furthermore, the micrograph also shows that the void space existing between the spheres is not preserved in the columnar thin film. These observations suggest that the top-most layer of the opal is acting as a template for the growth of the polymeric nanostructured film. Thus, the deposited organic materials consist in a hexagonal close packing arrangement of oriented organic nanopillars whose surface reproduce conformally the surface of the original opal substrate. Note that the original opal top-layer is integrated in the lower part of the cylindrical structures. The cylindrical nanopillars diameter are constant indicating a preferential growth perpendicular to the opal surface with a low lateral diffusion of the species (i.e., high sticking coefficients) arriving to the surface during the deposition. In any case, the reduced lateral growth produces the filling of the void space between the nanopillars generating the hexagonal tilling pattern observed in the polymeric surface (cf. Figure 1(b)). Additional effects responsible of the formation of the oriented nanostructured film are very likely shadowing effects and local inhomogeneities of the plasma sheath due to the opal surface topography.[31,32] This type of plasma nanostructured thin films has not being reported so far. Organic thin films grown simultaneously but using flat Si(100) and quartz substrates are continuous and uniform and present a very low surface roughness, as it has been observed in other films deposited by this technique.[28-31] Images illustrating the difference between the morphology of the film grown on an array of microspheres and on a flat substrate are provided as supporting information. It is interesting to notice that the structure herein presented has some similarities with non closed packed hexagonal patterns of hemispherical TiO_2 particles generated by pulsed laser deposition very recently reported.[33]

The sequential deposition of a second artificial opal (average sphere diameter 220 nm) onto the deposited organic layer yields a structure like the one shown in Figure 2. The periodic corrugation of the intermediate layer favours the growth of a second lattice of long range structural order, as seen in Figure 2(a). Furthermore, the relative orientation of the two crystals with respect to the original glass substrate is maintained. Similar structures were created using artificial opals made of spheres of different average diameter, with consistent results in all cases. Figures 2(b) and 2(c) display low magnification images of the cross section of organic planar defects sandwiched between two colloidal crystals made of 220 nm and 750 nm latex beads, respectively.

The level of accuracy and finesse with which the features of the substrate are reproduced by the PECVD technique employed can also be confirmed by observing the effect of the presence of a coating on the visible optical diffraction typically displayed by assemblies of microspheres of diameter larger than 400 nm. Pictures of the projection on a screen of the beams diffracted in the reflection medium by both an artificial opal made of 750 nm spheres and the same opal after being coated with a conformal layer of the organic fluorescent film are shown in Figures 3(a) and 3(b) respectively. A λ=532 nm laser line impinging normally on their surface was employed for this experiment. It can be seen how the pattern of spots on the screen remained unaltered after the conformal deposition of the luminescent organic layer, which further establishes that the corrugation of the periodic substrate is maintained. In fact, a certain narrowing of the diffraction spot area was observed after the deposition of the outer layer. This indicates that the divergence of the reflected diffracted beams potentially caused by the presence of imperfections in the opal lattice is reduced by effect of the outer conformal layer.

Breaking of the translational symmetry within photonic crystals gives rise to localized modes. This causes strong variations of the local photon density of states that may be reflected in both the opening of a transmission window in the forwardly forbidden band and, for the case of optically active materials, enhanced emission at wavelengths matching those resonant modes. Figures 4 (a) and 4(c) display the fluorescence spectra measured for 305 nm and 515 nm height luminescent organic layers, respectively, embedded within artificial opal films made of 220 nm diameter spheres. For the sake of comparison, the fluorescence spectrum measured from a 515 nm thick organic layer deposited on a stacking of 750 nm

diameter spheres, for which no photonic effects associated with a stop band at the dye emission frequencies were expected, is also shown. A photoemission enhancement factor γ is calculated for each case as the ratio between the fluorescence spectra of the photonic crystal sandwiched organic layer and the reference. For the opals films made of 220 nm diameter spheres the fluorescence intensity is higher in case of crystal containing thicker luminescent layer (515 nm thick). For the sake of comparison, fluorescent spectra are normalized at λ=650 nm, where no effect of the photonic structure is expected. Both samples were devised to assure that the lowest stop band of the photonic crystal coincides with the emission band of the solid dye slab, hence forcing any resonant modes due to the presence of a defect layer to overlap with part of such emission band. A transmission window can be clearly detected around λ=520 nm and λ=530 nm for the 305 nm and 515 nm thick defects, respectively. These reflectance dips at pseudogap frequencies are due to the presence of localized modes within the defect layers, for which the emission intensity is expected to be enhanced. Red-shadowed rectangles point out the spectral position of such localized modes. The enhancement effect was confirmed for both samples whose analysis is herein presented by comparing the spectral behaviour of γ with the specular normal reflectance spectrum measured in each case. In both cases, it can be clearly seen that γ peaks at those frequencies for which the resonance is detected in the reflectance spectrum. At the same time, it diminishes for those frequencies within the photonic stop band that are spectrally far from those localized modes. It should be remarked that for the sample used as reference no significant modification of the shape of the spectrum is observed with respect to that attained for the plane parallel dye slabs deposited onto flat substrates (Fig. S2). Reflectance spectrum of reference sample (Fig. S3) clearly shows that for this structure the lowest energy photonic pseudogap does not spectrally match the emission band of the organic layer. This proves that the variations of the shape of the emission band have a structural origin.

Results presented in Figure 4 demonstrate that by changing the deposition time it is possible to control the thickness of the organic layer acting as an optical dopant and thus tailor the spectral position of the localized mode it gives rise to. In Figure 5 we compare the experimental values of the defect state for

the two different intermediate layer thickness achieved with the theoretical predictions obtained using a scalar wave approximation.[35] Results are shown for defects embedded within lattices of 13 monolayers each. Experimental data are plotted as red crosses in Figure 5. As reported before,[20] the defect state sweeps the full width of the peak from the blue to the red end as the thickness of the defect increases, and repeats this behavior cyclically. The stop band edges estimated for the infinite crystal are depicted as horizontal dotted lines in Figure 5.

4. Conclusions

In summary, we have described a fast, reliable and accurate procedure to create two dimensional luminescent organic defect layers in artificial opals. A versatile room temperature remote plasma enhanced chemical vapour deposition has been used to create mechanically stable and non-soluble coatings. We have proven that the process yields a highly conformal growth that preserves the integrity and the properties of the polystyrene microspheres. The effect of resonant modes, caused by the presence of a middle layer in the photonic crystal, in both the reflectance and the photoemission spectra has been confirmed. Our work opens the possibility for integration of these nanostructures in purely organic light emitting devices in which the optical properties can be precisely controlled.

Acknowledgment. We thank the Spanish Ministry of Science and Innovation for funding provided under grants MAT2008-02166, MAT2007-65764, CONSOLIDER HOPE CSD2007-00007 and FUNCOAT 2010-CSD2008-00023, the Junta de Andalucía for grants FQM3579 and TEP2275 and EU contract nº 033793 (Phodye). GL thanks the Spanish Research Council for funding of his scholarship under the JAE program.

Supporting Information Available. Figure S1. FESEM image of a cross section of an edge of the photonic structure illustrating the different morphology of the dye layer attained when deposited on an array of spheres or on a flat substrate. Figure S2. Normalized absorbance and fluorescence spectra from a flat 3HF-adamantane plasma polymer film grew over quartz. Figure S3. Reflectance spectra obtained

from the sample employed as reference. This material is available free of charge via the Internet at http://pubs.acs.org.

Figure 1. FESEM images of the stages of the fabrication of a surface defect layer. (a) Top surface micrograph of the starting latex colloidal crystal film. (b) Top surface of the 2D planar defect layer. (c) Low-magnification micrograph of the cross-section showing the defect layer. (d) Detail of the defect layer. Scale bars are 1 μm in (a-c) and 500 nm in (d).

Figure 2. FESEM images of a defect layer embedded between two colloidal photonic crystal films. (a) Low-magnification micrograph showing that the 2D defect layer thickness is uniform over the whole sample. (b-c) Closer look to the defect layer. Opals shown in (a-b) are made of 220 nm polystyrene beads whereas those presented in (c) are made of 750 nm. Scale bar are 2 μm in (a) and 500 nm in (b-c).

Figure 3. Diffraction patterns of reflected beams projected on a screen parallel to the surface of the samples for λ=532 nm; (a) shows the diffracted beams exited from the surface of a colloidal crystal made of 750 nm diameter spheres, whereas (b) shows those emerged from a similar crystal covered by the conformal organic fluorescent layer.

Figure 4. Normalized fluorescent and reflectance spectra obtained from a 305 (a, b) and 515 nm (c, d) height defect layer embedded within two artificial opal films made of 220 nm diameter spheres. (a, c) Normalized fluorescence spectra of the layer embedded within a photonic crystal (red line) and of a 515 nm thick organic layer deposited on a stacking of 750 nm diameter spheres, for which no photonic effects associated with a stop band at the dye emission frequencies were expected (black line). (b, d) Reflectance spectrum of the defect layer sandwiched between the two colloidal crystal films and the enhancement factor γ, defined as the ratio between the fluorescence spectra presented in (a, c). Red dotted line represents γ=1 line.

Figure 5. Theoretical dependence between the localized mode associated to the defect state and the thickness of the organic fluorescent layer. Experimental values extracted both from the FESEM characterization and from the fittings of the reflectance spectra presented in Figure 4 (b-d) are plotted as red crosses. Horizontal dotted lines depict the stop band limits of the infinite crystal.

A general method to introduce solid organic luminescent planar defects within artificial opals is herein presented. Sequential conformal growth of colloidal crystals by convective self-assembly and slabs of a purely organic dyed matrix, attained by low temperature remote plasma enhanced deposition, gives rise to heterostructures like the one whose cross section is shown in the upper picture, in which the colloidal crystals are made of polystyrene spheres (scale bar is 2μm). The luminescent organic layer behaves both as an optical dopant, causing the opening of transmission windows within the forbidden frequency interval of the lattice (black curve in lower figure), and as an optically active material, whose emission (red curve in lower figure) can be tailored by the photonic environment.

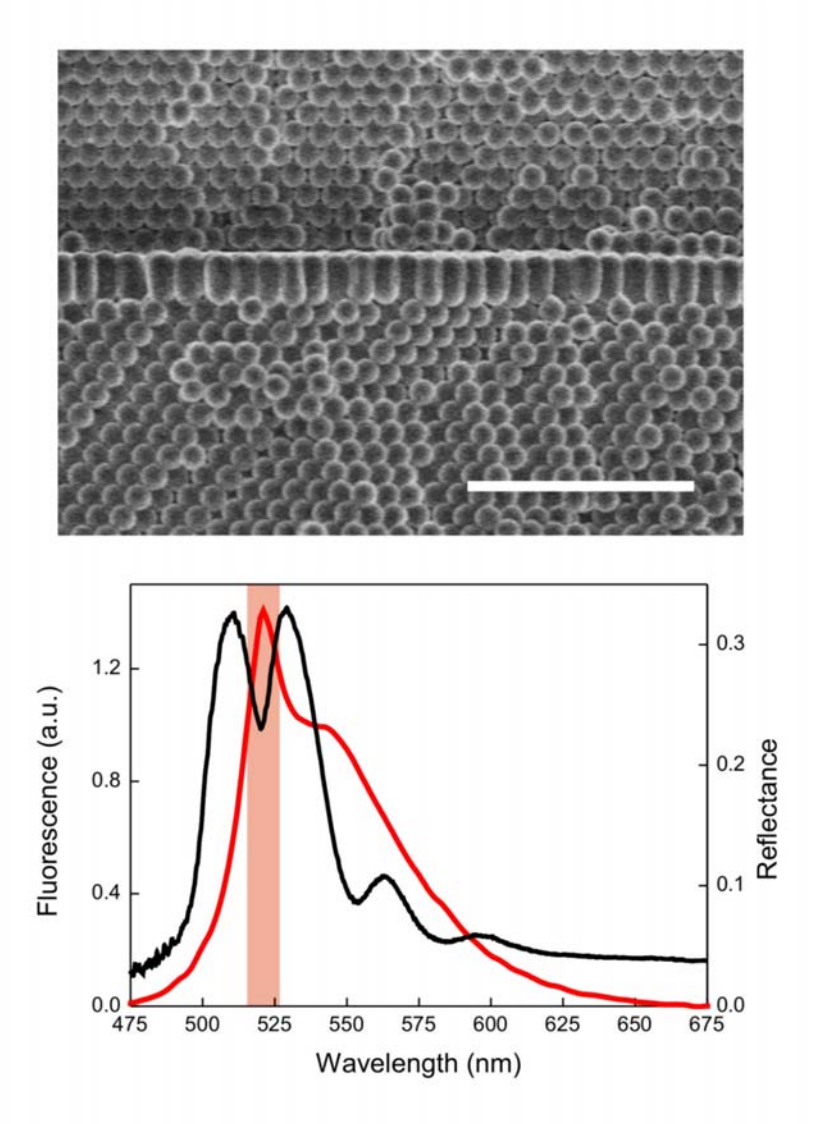

Graphical T.O.C. F. J. Aparicio *et al*.

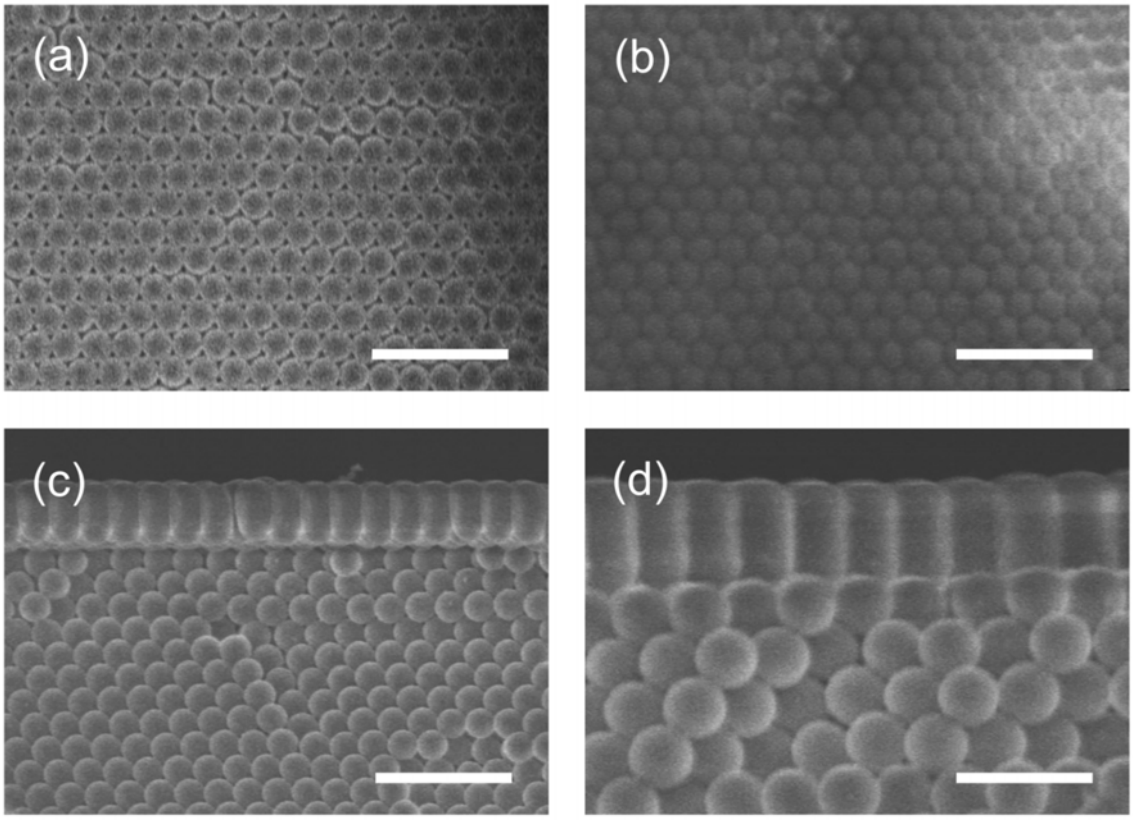

Figure. 1. F. J. Aparicio *et al*.

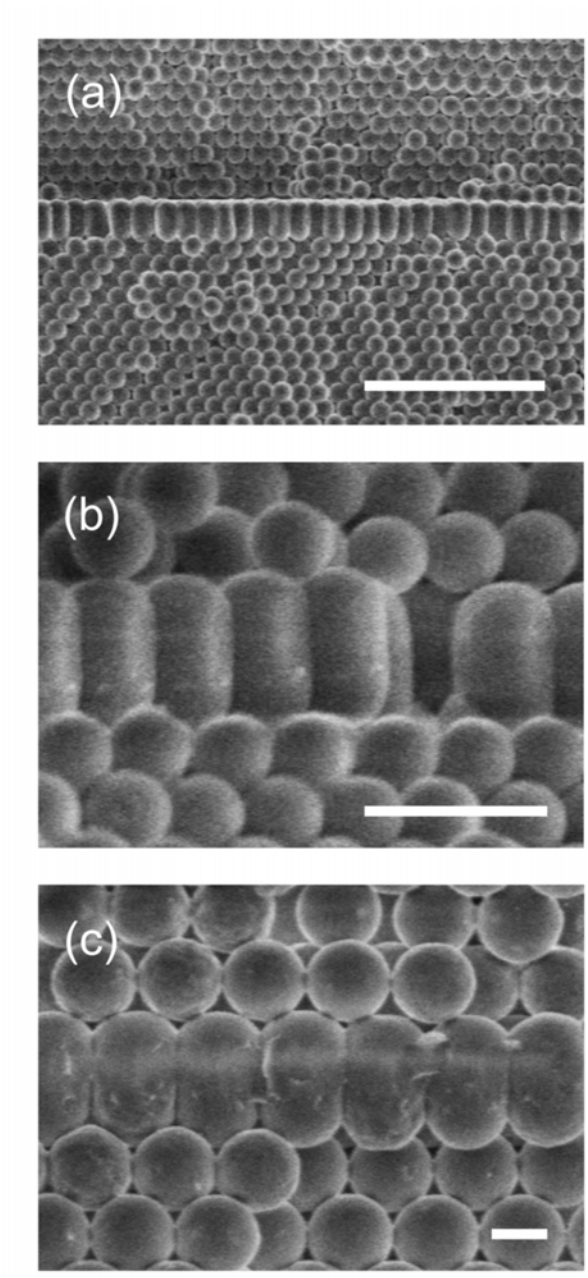

Figure. 2. F. J. Aparicio *et al*.

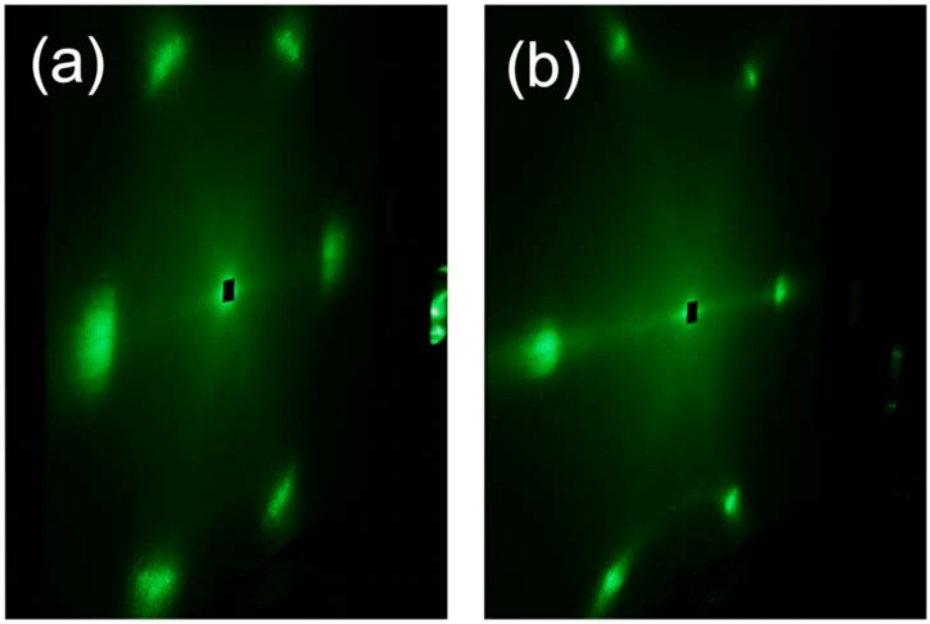

Figure. 3. F. J. Aparicio *et al*.

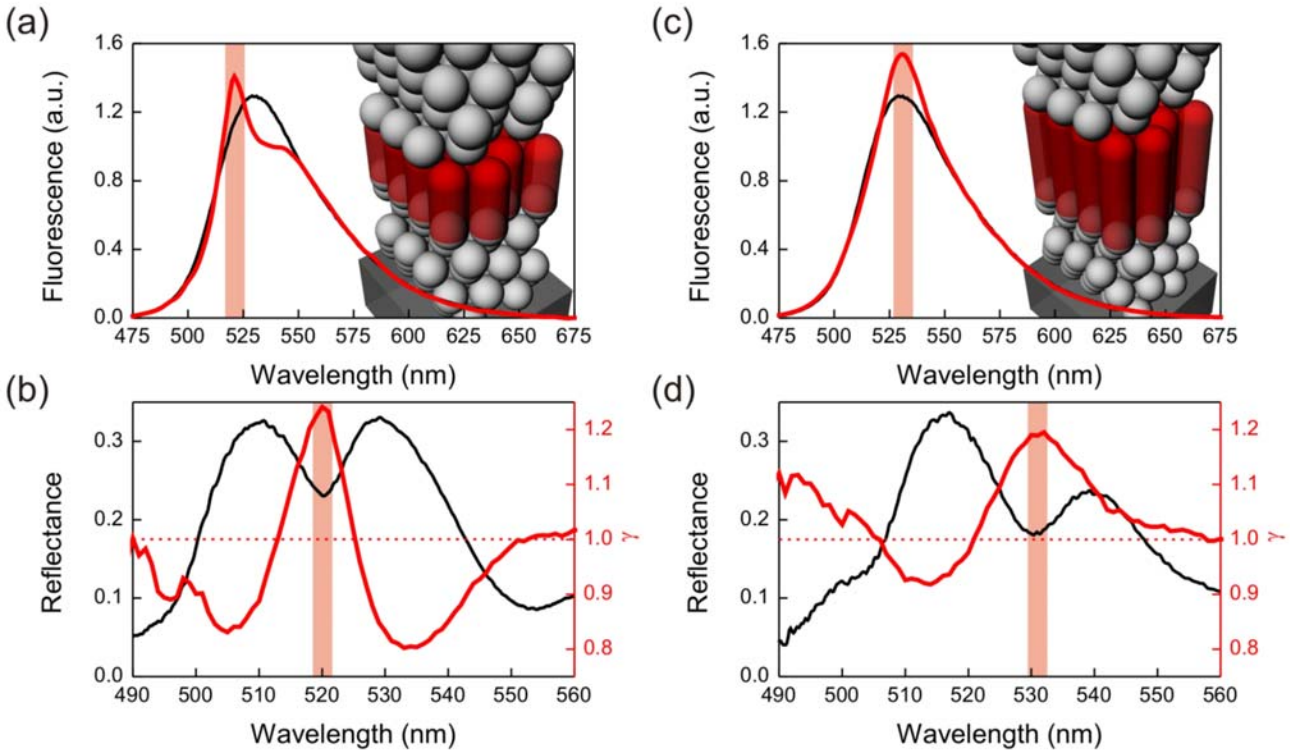

Figure. 4. F. J. Aparicio *et al*.

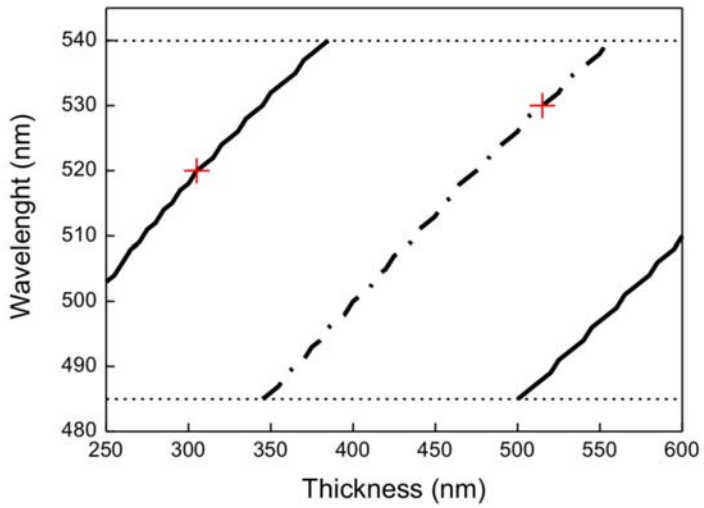

Figure. 5. F. J. Aparicio *et al*.

(1) Yablonovitch, E.; Gmitter, T.J.; Meade, R.D.; Rappe, A.M.; Brommer, K.D.; Joannopoulos, J.D. *Phys. Rev. Lett.* **1991**, *67*, 3380.

(2) Joannopoulos, J. D.; Villeneuve, P. R.; Fan, S. *Nature* **1997**, *386*, 143.

(3) Jiang, P.; Bertone, J. F.; Hwang, K. S.; Colvin, V. L. *Chem. Mater.* **1999**, *11*, 2132.

(4) Lee, W.; Pruzinsky, S.A.; Braun, P.V. *Adv. Mater.* **2002**, *14*, 271.

(5) Arsenault, A.; Fleischhaker, F.; von Freymann, G.; Kitaev, V.; Míguez, H.; Mihi, A.; Tétreault, N.; Vekris, E.; Manners, I.; Aitchison, S.; Perovic, D.; Ozin, G. A. *Adv. Mater.* **2006**, *18*, 2779.

(6) Braun, P. V.; Rinne, S. A.; García-Santamaría, F. *Adv. Mater.* **2006**, *18*, 2665.

(7) Yang, Q.; Wang, L.; Zhao, X. S. *Adv. Funct. Mater.* **2007**, *17*, 3695.

(8) Tétreault, N.; Míguez, H.; Yang, S.M.; Kitaev, V.; Ozin, G.A. *Adv. Mater.* **2003**, *15*, 1167.

(9) Juárez, B.H.; Golmayo, D.; Postigo, P.A.; López, C. *Adv. Mater.* **2004**, *16*, 1732.

(10) Jonsson, F.; Sotomayor Torres, C. M.; Seekamp, J.; Schniedergers, M.; Tiedemann, A.; Ye, J.; Zentel, R. *Microelectron. Eng.* **2005**, *429*, 78.

(11) Vekris, E.; Kitaev, V.; von Freymann, G.; Perovic, D.D.; Aitchison, J.S.; Ozin, G.A. *Adv. Mater.* **2005**, *17*, 1269.

(12) Yan, Q.F.; Zhou, Z.C.; Zhao, X.S.; Chua, S.J. *Adv. Mater.* **2005**, *17*, 1917.

(13) Jun, Y.H.; Leatherdale, C.A.; Norris, D.J. *Adv. Mater.* **2005**, *17*, 1908.

(14) Blanco, A.; Chomski, E.; Grabtchak, S.; Ibisate, M.; John, S.; Leonard, S. W.; López, C.; Meseguer, F.; Míguez, H.; Mondia, J. P.; Ozin, G.A.; Toader, O.; van Driel, H.M. Nature **405**, 437 (2000).

(15) Vlasov, Y.A.; Bo, X.Z.; Sturm, J.C.; Norris, D.J. *Nature* **2001**, *414*, 289.

(16) Rinne, S. A.; García-Santamaría, F.; Braun, P. V. *Nature Photonics* **2008**, *2*, 52.

(17) Zhao, Y.; Wostyn, K.; de Schaetzen, G.; Clays, K.; Hellemans, L.; Persons, A.; Szekeres, M.; Schoonheydt, R.A. *Appl. Phys. Lett.* **2003**, *82*, 3764.

(18) Míguez, H.; Tetreault, N.; Hatton, B.; Yang, S.M.; Perovic, D.; Ozin, G.A. *Chem. Comm.* 2002, 2736.

(19) Palacios-Lidón, E.; Galisteo-López, J. F.; Juárez, B. H.; López, C. *Adv. Mater.* 2004, *16*, 341.

(20) Tétreault, N.; Mihi, A.; Miguez, H.; Rodriguez, I.; Ozin, G.A.; Meseguer, F.; Kitaev, V. *Adv. Mater.* **2004**, *16*, 346.

(21) Pozas, R.; Mihi, A.; Ocaña, M.; Míguez, H. *Adv. Mater.* **2006**, *18*, 1183.

(22) Fleischhaker, F.; Arsenault, A.C.; Schmidtke, J.; Zentel, R.; Ozin, G.A. *Chem. Mater.* **2006,** *18,* 5640.

(23) Galisteo-López, J. F.; Galli, M.; Andreani, L. C.; Mihi, A.; Pozas, R.; Ocaña, M. Míguez, H. *Appl. Phys. Lett.* **2007**, *90*, 101113.

(24) Tétreault, N.; Arsenault, A.C.; Mihi, A.; Wong, S.; Kitaev, V.; Manners, I.; Míguez, H.; Ozin, G.A. *Adv. Mater.* 2005, *17*, 1912.

(25) Furumi, S.; Fudouzi, H.; Miyazaki, H. T.; Sakka, Y. *Adv. Mater.* **2007**, *19*, 2067.

(26)Yasuda, H., Luminous Chemical Vapor Deposition and Interface Engineering, CRC: **2004**

(27) García-Santamaría F.; Miyazaki, H.T.; Urquia, A; Ibisate, M.; Belmonte, M.; Shinya, N.; Meseguer, F.; López C. *Adv. Mater.* **2002**, *14*, 1144.

(28) Barranco, A.; Groening, P. *Langmuir* **2006**, *22*, 6719.

(29) Barranco, A.; Aparicio, F.J.; Yanguas-Gil, A.; Groening, P.; Cotrino, J.; González-Elipe, A.R. *Chem. Vap. Deposition* **2007**, *13*, 319.

(30) Blaszczyk-Lezak, I.; Aparicio, F.J.; Borrás, A.; Barranco, A.; Álvarez-Herrero, A.; Fernández-Rodriguez, M.; González-Elipe, A.R. *J. Phys. Chem. C*, **2009**, *113*, 431.

(31) Ostrikov, K. *Rev. Mod. Phys.* **2005**, *77*, 489.

(32) Borrás, A.; Barranco, A.; Espinós, J.P.; Cotrino, J.; Holgado, J.P.; González-Elipe, A.R. *Plasma Proc. Polym.* **2007**, *4*, 515.

(33) Li, Y.; Sasaki, T.; Shimizu, Y.; Koshizaki, N. *Small* **2008**, *4*, 2286.